Journal of Catalysis **193,** 273–282 (2000)
doi:10.1006/jcat.2000.2900, available online at http://www.idealibrary.com on IDEAL®

A Model for the Temperature-Programmed Reduction of Low and High Surface Area Ceria

Francesca Giordano,* Alessandro Trovarelli,† Carla de Leitenburg,† and Massimiliano Giona*

*Dipartimento di Ingegneria Chimica e Materiali, Università di Roma La Sapienza, via Eudossiana 18, 00184 Rome, Italy; and †Dipartimento di Scienze e Tecnologie Chimiche, Università di Udine, via Cotonificio 108, 33100 Udine, Italy
E-mail: trovarelli@dstc.uniud.it

Received December 24, 1999; revised April 10, 2000; accepted April 11, 2000

This article develops an experimental and theoretical kinetic analysis of ceria reduction using TPR experiments, considering both low and high surface area samples. From data in the existing literature on oxygen diffusion within the ceria lattice, it may be shown that spatial effects within ceria crystallites can be neglected for temperature ranges relevant to ceria reduction without risking significant errors. Moreover, oxygen transport seems not to be responsible for the qualitative changes in TPR profiles occurring on low and high surface area samples. We have developed a simple kinetic model that is able to predict the unimodal and bimodal shape of low and high surface area ceria with correct location of the main peaks. The model displays a satisfactory quantitative agreement with respect to the degree of reduction as a function of temperature. The model highlights the influence of the kinetic and thermodynamic properties of the material and of its textural changes with temperature (sintering). The model can be used to predict the outcome of TPR experiments over a broad range of specific surface areas.

Key Words: **ceria; CeO_2; temperature-programmed reduction; TPR; oxygen storage capacity; redox behavior; oxygen diffusion.**

1. INTRODUCTION

A great number of studies have appeared in recent years on the reduction behavior of ceria and related materials, as a result of their use as a redox/oxygen storage component in the formulation of three-way catalysts (1–7). To carry out this action, ceria must be able to take up and release oxygen following variations in the feedstream stoichiometric composition. In doing so, during the operation, the catalyst is continuously subjected to reduction and oxidation involving alternating creation and removal of oxygen vacancies. The dynamic controlling this redox process is rather complex and may depend on both kinetic and thermodynamic constraints. It is therefore important to improve understanding of the factors that may affect the reduction process and to develop kinetic models that can describe and predict the process.

A simple, and quite useful, method for obtaining information on the steps involved in these processes is temperature-programmed reduction (TPR), which simply analyzes the reduction profile as a function of temperature. The first TPR on ceria dates back to 1980 (8), but only a few years later was it first suggested that reduction in ceria may follow a two-stage process (9). Typically, the reduction profile of CeO_2 shows two peaks. The first, low-temperature, signal located at ca. 770 K was assigned to the reduction of the most easily reducible surface-capping oxygen of ceria, while removal of the bulk oxygens was suggested as the cause of the high-temperature signal at ca. 1100 K. Similar correlations were reported later by others, who found a good relationship between BET surface area and H_2 consumption at low temperature (2, 10, 11). Attempts were also made to rationalize data to calculate the surface area from TPR traces, although their validity has been questioned and is restricted to narrow surface area ranges (12). Reduction processes operated by H_2 under stationary conditions also suggested that surface steps were rate limiting. El Fallah *et al*. developed a model for the reduction of pure ceria by taking into account both surface and bulk steps and found that hydrogen dissociation is the limiting step in the surface process on pure ceria (4). The stepwise reduction of ceria, involving the surface and the bulk at different stages, is also confirmed by theoretical analysis of surface/bulk reduction energies (13, 14) and by the measurement of defect thermodynamics (15, 16), which indicates that high surface area nanocrystalline ceria has a lower reduction enthalpy than that measured for the bulk material.

To elucidate this topic, with previous findings in mind, we develop here for the first time a simple quantitative model for the TPR profile of ceria which can explain the origin of the two different peaks in the reduction traces, suggesting a participation of surface and bulk oxygen in the reduction process at low and high temperature, respectively. It is shown that the profile can be reproduced by assuming a surface kinetic control over the entire temperature range, although a knowledge of the thermodynamics of bulk reduction is necessary to model the profile at high temperature, where the reduction process occurs not too far from equilibrium conditions. Interestingly, it will also be shown that

0021-9517/00 $35.00

for pure ceria, diffusion at $T > 650$ K is fast and does not limit bulk reduction at high temperature.

2. EXPERIMENTAL APPARATUS AND SETUP

Materials

High surface area cerium oxide (HSA-CeO_2, 44 $m^2\ g^{-1}$) was obtained from Grace Davison (sample 18424-171-A). Sample purity was 99.78% with traces of La_2O_3 (0.07), MgO (0.04), P_2O_5 (0.02), and ZrO_2 (0.02). Low surface area ceria (LSA-CeO_2, 3 $m^2\ g^{-1}$) was purchased from Janssen (lot 06759/3, sample purity 99.9%). The samples were treated at 773 K for 1 h under an O_2/He 20/80 v/v atmosphere before TPR measurements.

Methods

Temperature-programmed reduction (TPR) was performed in a conventional, U-shaped, quartz microreactor (i.d. = 6 mm, $l = 200$ mm) using a 5% H_2 in argon mixture flowing at 35 $cm^3\ min^{-1}$ (STP). For TPR measurements, the temperature range investigated was 295–1400 K and the heating rate was always 10 K min^{-1}. The reduction of CuO to metallic copper was used to calibrate the TPR apparatus for H_2 consumption. BET surface areas were measured with a Carlo Erba Sorptomatic 1900 instrument.

3. RESULTS AND DISCUSSION

3.1. TPR Profiles and the Effect of Oxygen Diffusion

The results of typical TPR experiments performed on both low and high surface area CeO_2 samples (henceforth LSA and HSA, respectively) are depicted in Fig. 1. The typical profile corresponding to LSA ceria is characterized by a single peak centered at $T = 1100 \pm 10$ K. The intensity of the peak depends on operating conditions, such as the weight of the sample or the hydrogen flow rate, whereas its location (i.e., the temperature corresponding to the local maximum) is an intrinsic feature of ceria reduction, since it depends on the material and is less affected by variations in the operating conditions.

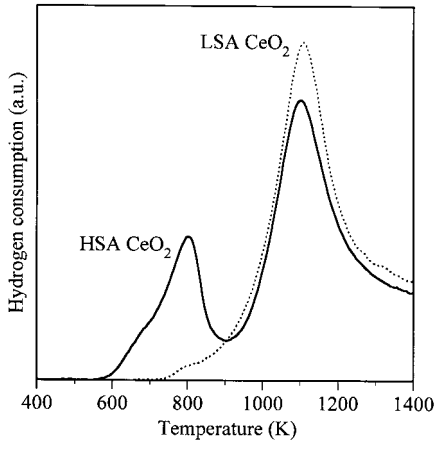

FIG. 1. Experimental H_2 conversion, expressed in arbitrary units, obtained by TPR experiments performed on LSA (3 $m^2\ g^{-1}$) and HSA (44 $m^2\ g^{-1}$) ceria.

The TPR profiles of HSA ceria are characterized by the presence of two peaks (bimodal curve). The high-temperature peak preserves the temperature location observed in the case of LSA ceria, thus showing that this peak in TPR profiles is intrinsic to the material. The intensity of the second peak is slightly less than in the case of LSA samples because a fraction of ceria has been already reduced at lower temperatures (we analyze this feature in Section 3.3). The first peak is located at a temperature of 770 ± 10 K, independently of the sample, whereas its shape in detail closely depends on the preparation conditions (duration and temperature of thermal pretreatments to remove impurities) the material has undergone before TPR. This variability in the shape may be due to variations in specific area (which are more significant for HSA samples) and to the presence of surface impurities in the material (17), such as carbon monoxide and dioxide, which reach the detector after desorption. Further complications may be caused by the storage in bulk ceria during reduction of some H_2, which is then released at higher temperatures (18).

TPR of ceria, like that of any other material, depends on four main effects, the thermodynamics and kinetics of reduction, the textural changes (sintering) the material undergoes with temperature, and diffusion phenomena within the material, which in the case of ceria means oxygen diffusion in the lattice structure (19). In the light of the modeling of the TPR dynamics, it is important to ascertain the effects of each of these phenomena on the evolution of the process. We discuss here the latter two effects, leaving to Sections 3.2 and 3.3 a thorough analysis of thermodynamic and kinetic properties.

It is entirely reasonable to suppose that oxygen diffusion within the ceria lattice structure may influence the shape of TPR profiles. By assuming this to be true as a working hypothesis, the bimodal shape observed in HSA samples could be attributed to a reduction in the surface ceria at low temperature, giving rise to the first peak around 770 K, and a subsequent reduction with oxygen supplied from the bulk at higher temperatures. In this conceptual framework, the two-peak shape of HSA ceria would be a consequence of the diffusional resistance associated within oxygen surface diffusion.

The features of oxygen migration in pure and doped ceria have been the subject of several studies (21), and diffusion coefficients are available in the literature, albeit in temperature ranges which are relatively narrow compared to current TPR experiments (20–23). The oxygen diffusion coefficient $D(T)$ can also be recovered from

measurements of ionic conductivity σ_i, by enforcing the Nernst–Einstein relation (21). Temperature dependence of $D(T)$ can be expressed by the Arrhenius equation $D(T) = D_0 \exp(-E_D/k_B T)$, typical of activated processes, and the values of the preexponential factor D_0 and of the activation energy E_D can be extrapolated from the literature data (24), although their validity is limited to specific temperature ranges.

A simple order of magnitude analysis of these data demonstrates that diffusion, although necessary for the reaction to occur, is not a limiting phenomenon at temperatures significant for TPR experiments. For this purpose, let us consider the characteristic diffusion length $l_d(T)$ expressed as

$$l_d(T) = \sqrt{2D(T)t(T)}, \qquad [1]$$

where $t(T) = (T - T_0)/\beta$, β being the heating rate and T_0 the initial temperature. This quantity is to be compared with the characteristic geometric linear size of ceria crystallites, which can be evaluated by $l_c(T) = \epsilon V_c/A(T)$, V_c being the volume of the sample, ϵ being a constant depending on the geometry of ceria crystallites (for example $\epsilon = 1/6$ for cubic crystallites), and $A(T) = \alpha(T)m$ being the overall surface area, i.e., the product of the specific surface area $\alpha(T)$ times the mass m of the sample. A discussion of the shape of the specific surface area $\alpha(T)$ versus T is postponed until Section 3.3. Figure 2 depicts $l_d(T)$ and $l_c(T)$ as functions of temperature for the different sets of experimental data for $D(T)$ obtained by several authors (20, 22, 24). It can be observed that $l_d(T)$ is definitely greater than $l_c(T)$ for $T > 650$ K, that is to say, for the temperatures at which the reaction occurs at a significant rate, as can be seen from the TPR data of Fig. 1 in the case of LSA ceria. This result has an important implication. It can be concluded that diffusion is not limiting for the reduction of LSA samples. This is in agreement with recent findings reported by Fornasiero *et al.*, who showed that H_2 activation is rate limiting in the reduction process at high temperature on pure ceria (25). In the case of HSA materials, a slight effect of diffusion might be observed at the lowest temperatures, 400–650 K, whereas for higher temperatures such effects can be ignored as for LSA samples. This implies, for modeling purposes, that the degree of reduction can be assumed to be uniform over the entire sample or, more specifically, that TPR kinetics can be described by concentration variables (degree of reduction) exclusively dependent on time and not on a spatial variable parametrizing the position within each cristallite or pellet. Moreover, and this is essentially the most important conclusion, Fig. 2 indicates that oxygen transport within ceria crystallites cannot be consider the factor influencing the qualitative changes in TPR profile observed in low and high surface area ceria depicted in Fig. 1.

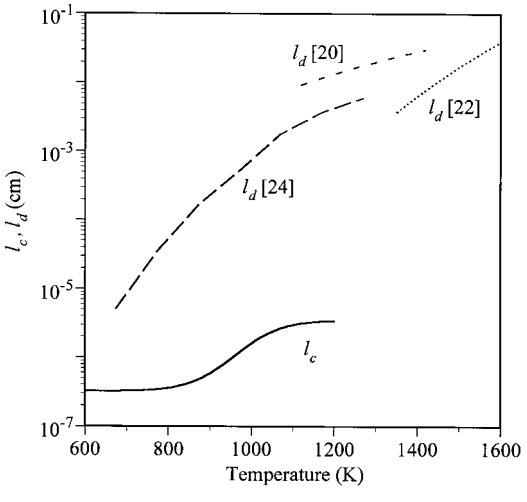

FIG. 2. Geometric linear size of ceria crystallites l_c versus temperature for sample with initial specific area of 44 $m^2 g^{-1}$, compared to characteristic diffusional length scale l_d given by Eq. [1] for several experimental data for oxygen diffusion coefficient D available in the literature (Refs. (24), (20), (22)), plotted within the range of experimental validity.

Let us now consider textural changes as the reduction proceeds. BET measurements performed on samples reduced at different temperatures under conditions similar to those of TPR indicate that HSA ceria undergoes sintering with a reduction in surface area up to two orders of magnitude. The drop in surface area in H_2-rich atmospheres is greater than that observed under oxidizing or inert atmospheres, and this is in agreement with previous studies (26) (see also Fig. 6). The surface area decay due to sintering is localized in a narrow temperature range ~(600, 1050): at $T = 1100$ K, the sample has lost most of its surface area. Therefore, for temperatures higher than 1000–1050 K, the behavior of HSA ceria is analogous to that of an LSA sample. The sintering process is significant in the temperature ranges corresponding to the occurrence of the first TPR peak, and it can be argued that sintering is essential to describe the reduction dynamics of HSA ceria.

We may conclude this qualitative and semiquantitative analysis by observing that oxygen diffusivity in TPR experiment temperature ranges is sufficiently high to consider the reduction degree homogeneous within the ceria sample, and that the differences observed for LSA and HSA ceria should be attributed to the interplay between thermodynamic and kinetic properties and textural changes due to sintering. In the light of these results, the next two subsections will focus on the kinetic modeling of LSA and HSA ceria separately.

3.2. Kinetic Model of LSA Ceria Reduction

In order to model the thermodynamics of ceria reduction under H_2, the two sets of reactions and their corresponding equilibrium data must be used,

$$CeO_2 \rightleftharpoons CeO_{1.5} + 0.25O_2 \qquad [2]$$

$$H_2 + 0.5O_2 \rightleftharpoons H_2O, \qquad [3]$$

which give

$$2CeO_2 + H_2 \rightleftharpoons 2CeO_{1.5} + H_2O. \quad [4]$$

Data for equilibrium [4] can be calculated from Ref. (27) provided that the partial pressure ratio p_{H_2}/p_{H_2O} is available. Unfortunately, the real partial pressure ratio above the surface under TPR conditions is not known. Therefore, we preferred to obtain insight into reduction dynamics by considering modified temperature-programmed experiments (MTPR for short). In these experiments, the linear temperature rise is stopped at a fixed value T_s, and the material undergoes further reduction under isothermal conditions at temperature T_s. The system is left to evolve until hydrogen concentration saturates to the inlet value (i.e., no further reduction occurs). Such experiments aim to identify the main phenomena governing ceria reduction, namely, the thermodynamic and kinetic aspects. Moreover, as we will show below, these experiments are very useful for a quantitative estimate of the thermodynamic/kinetic properties of reduction.

Figure 3A depicts several MTPR profiles as a function of the time elapsing from the beginning of the experiment for different values of T_s in the range (960, 1200) K. For $t < t(T_s)$ ($t(T_s)$ being the instant at which $T = T_s$ and the temperature rise is stopped), the profile is identical to that of a standard TPR. For $t > t(T_s)$, hydrogen consumption (proportional to the rate of reduction) displays a more or less sudden decay to zero, depending on temperature T_s. The decay is very sudden for high values of T_s above 1100 K, and it is much slower for temperatures below 1000 K. For this reason, in order to enhance the graphical representation, the curve corresponding to $T_s = 961$ K in Fig. 3A has been represented over time scales much lower than those necessary to reach a vanishing hydrogen consumption.

The integral of an MTPR profile is proportional to the equilibrium value of the reduction degree at temperature, T_s, which can be quantitatively inferred upon calibration.

In this way, by comparing the MTPR and the standard TPR profiles, thermodynamic and kinetic effects can be separated and estimated quantitatively. To this end, it is convenient to display TPR and MTPR data in a graph expressing the reduction degree x (corresponding to a final material with composition CeO_{2-x}) vs time as in Fig. 3B. This figure highlights that the reduction degree in an MTPR approaches a saturation value asymptotically corresponding to the equilibrium condition at T_s. The equilibrium data ($x_{eq}(T_s)$ vs T_s) can be reasonably approximated by the empirical expression

$$x_{eq}(T) = \frac{T - T_{r1}}{c_1(1 + a_1 \exp(b_1/(T - T_{r1})))},$$

whose constant parameters T_{r1}, a_1, b_1 and c_1 are listed in Table 1. Experimental equilibrium data for temperatures greater than $T = 1200$ K are not available, because of the practical difficulty of maintaining controlled experimental conditions at high temperatures for long time, that is, for the time necessary to reach equilibrium conditions. The experimental setup would be subject to excessive thermal stresses and the results would subsequently be unreliable. For this reason, the above-mentioned empirical equation for $x_{eq}(T)$ is to be considered as a linear extrapolation of the main trend of experimental equilibrium conversions appearing in the range 1100–1200 K.

A compact and efficient graphical representation of equilibrium and kinetic TPR results is given in Fig. 4. It may be observed that the equilibrium reduction degree of LSA ceria at $T = 1400$ K is slightly less than $x = 0.25$ (that is, to a ceria composition $CeO_{1.75}$), which corresponds to 50% of the maximum attainable reduction.

Let us now analyze the modeling assumption leading to a simple quantitative characterization of the reduction

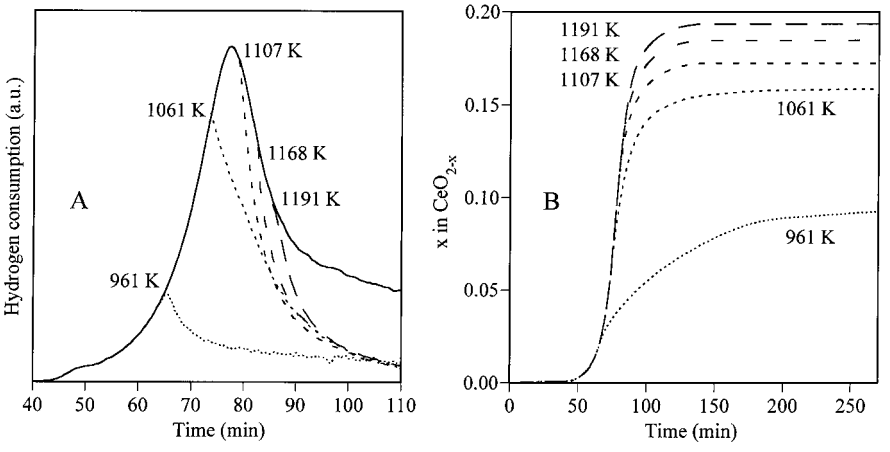

FIG. 3. (A) Experimental MTPR profiles plotting H_2 conversion (a.u.) versus time (min) for LSA ceria with different T_s. (B) Experimental reduction degree x in CeO_{2-x} versus time attained in MTPR experiments on LSA ceria at different values of T_s.

TABLE 1

List of Model Parameters, Obtained by Fitting Experimental Data

Symbol	Value	Units
a_1	1.0×10^{-10}	dimensionless
b_1	16500	K
c_1	5000	K
T_{r1}	220	K
a_3	6.39×10^{-7}	dimensionless
a_4	1.3×10^{-7}	dimensionless
b_3	3.2×10^{-3}	K^{-1}
b_4	15500	K
T_{r3}	80	K
$\bar{a}_3$	1.55×10^{-7}	dimensionless
$\bar{a}_4$	5.0×10^{-7}	dimensionless
$\bar{b}_3$	1.65×10^{-3}	K^{-1}
$\bar{b}_4$	8900	K
$\bar{T}_{r3}$	50	K

kinetics. To model TPR dynamics, we assume that the system is formed by two pseudo-species, namely, CeO_2 and $CeO_{1.5}$, the former representing the unreduced ceria and the latter the oxide at the maximum admissible degree of reduction, i.e., $x_{max} = 0.5$. This, of course, does not represent the real situation where a continuum of nonstoichiometric suboxides of composition CeO_{2-x} $(0 \le x \le 0.5)$ exists over most of the reduction range, but it is a good model to represent the actual degree of reduction as a function of two species only.

The reduction can be expressed by the reversible reaction

$$CeO_2 \rightleftharpoons CeO_{1.5} + \frac{1}{4}O_2. \qquad [5]$$

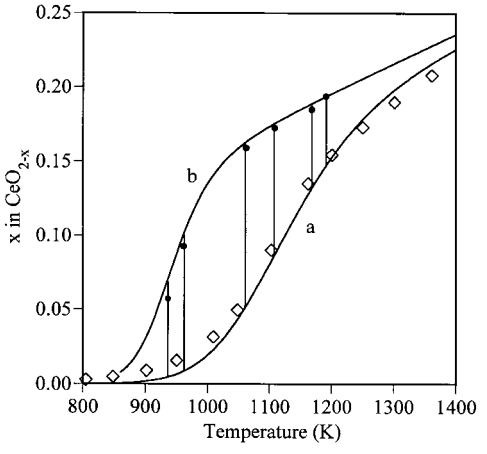

FIG. 4. Experimental and theoretical reduction degree x in CeO_{2-x} versus T for LSA ceria. Curve (a) is a simulated $x(T)$ curve (obtained from model), compared with corresponding experimental data obtained by TPR experiments, plotted with diamonds (◇). Curve (b) is an equilibrium curve $x_{eq}(T)$ passing through experimental equilibrium points (●), evinced from saturation values attained in MTPR experiments. These values should be compared with the theoretical results plotted with vertical lines at the following values of T_s: 936, 961, 1061, 1107, 1168, and 1191 K.

With this representation, the actual degree of reduction can be appropriately expressed in terms of the dimensionless variable

$$z = \frac{[CeO_{1.5}]_T}{[CeO_2]_{T_0}}, \qquad [6]$$

attaining values between 0 and 1, $[CeO_{1.5}]_T$ being the concentration of the completely reduced oxide at a generic temperature T and $[CeO_2]_{T_0}$ being the initial concentration of the unreduced material at the beginning of the experiment (since $[CeO_{1.5}]_{T_0} = 0$). It is easy to see that $z = 2x$.

Since it has been shown in a previous section that oxygen bulk diffusion is never limiting in the reduction-significant range of temperatures, $z = z(t)$ (or equivalent function of T) is spatially homogeneous. The kinetics of reduction can thus be expressed by the differential equation

$$V_c \frac{dz}{dt} = k_1(T) A_0 (1 - z) - k_2(T) A_0 z p_{O_2}^{1/4}, \qquad [7]$$

which corresponds to the assumption that Eq. [5] is an elementary reaction. In Eq. [7], V_c is the sample volume, A_0 is the surface area available for the reaction (which is constant for LSA ceria), and $k_1(T)$ and $k_2(T)$ are the kinetic rate coefficients of the forward and reverse reactions in Eq. [5], respectively. Moreover, it can be assumed that the oxygen partial pressure equals its equilibrium value at any temperature T, bringing it within the temperature dependence of $k_2(T)$. Thus, by introducing the dimensionless variable $\theta = t/\tau_p$, where τ_p is the reactor residence time, and after some algebra, the dimensionless form of Eq. [7] reads

$$\frac{dz}{d\theta} = \tilde{k}_1(T)\left(1 - \frac{z}{z_{eq}(T)}\right) \qquad [8]$$

with the initial condition $z(\theta = 0) = 0$. The temperature-programmed profile is given by $T(\theta) = T_0 + \beta\tau_p\theta$, where β is the rate of programmed temperature rise ($K\ s^{-1}$).

In Eq. [8] we have made use of the symbols $\tilde{k}_1(T) = k_1(T) A_0 \beta \tau_p / V_c$ and $z_{eq}(T) = 2x_{eq}(T)$. The latter quantity can be experimentally obtained from MTPR data (see Fig. 3B). The temperature dependence of the kinetic rate coefficient $\tilde{k}_1(T)$ can be directly obtained from the experimental data, by substituting into Eq. [8] the expression for $z_{eq}(T)$ and by evaluating $z(T) = 2x(T)$ from the experimental data of a standard TPR profile.

This approach yields an expression for the kinetic coefficient $\tilde{k}_1(T)$ which can be approximated from the relation

$$\tilde{k}_1(T) = \frac{a_3 \exp(b_3 T)}{(1 + a_4 \exp(b_4/(T - T_{r3})))},$$

which corresponds to a modulation of a standard Arrhenius dependence. The parameters in this expression are reviewed in Table 1.

To complete the model, let us consider the gas-phase reaction $H_2 + 1/2O_2 \rightarrow H_2O$, since the experimental data

associated with the TPR profile are proportional to hydrogen concentration. If we assume that no resistance to mass transfer is offered by the material or the gas phase, the balance equation for the hydrogen concentration in the gas phase within the differential reactor setup reads

$$V_r \frac{dc_{H_2}}{dt} = F\left(c^0_{H_2} - c_{H_2}\right) - V_r r_{H_2}, \qquad [9]$$

with the initial condition $c_{H_2}(0) = c^0_{H_2}$. In this equation, V_r represents the reactor volume, F the volumetric flow rate, and r_{H_2} the specific rate of hydrogen consumption. It may be observed after stoichiometry that the hydrogen consumption rate equals the specific rate of ceria reduction, expressed with respect to the z variable; that is, r_{H_2} equals the right-hand side of Eq. [7].

Equation [9] can be rewritten in dimensionless form by introducing the variable $y = c_{H_2}/c^0_{H_2}$,

$$\frac{dy}{d\theta} = 1 - y - \tilde{k}_1(T)\frac{1}{2}\frac{\gamma}{\delta}\left(1 - \frac{z}{z_{eq}(T)}\right), \quad y(0) = 1, \qquad [10]$$

where γ is the ratio of the initial concentration of ceria and hydrogen, and $\delta = V_r/V_c$. Table 1 reviews the values of the dimensionless parameters in the balance equations, Eqs. [8]–[10], corresponding to the experimental conditions used in the present work. By integrating these equations, the value of $1-y$ can be obtained, which is proportional to the experimental measurements by a conductance probe of the TPR profile. To compare the results of the model and the experimental data, we shall consider Fig. 5, in which the profiles have been normalized on a common basis for a clearer visualization. It can be observed that the simulated TPR is in very good agreement with the experimental profile in its main features, represented by the peak location and by the asymmetric profile, with a slower tail for temperatures greater than the peak temperature. The uncertainty in the high-temperature equilibrium data highlighted above may be responsible for the slightly higher values of hydrogen conversion with respect to the experimental values at those temperatures. At this point, we should stress the importance of thermodynamic data in modeling the high-temperature TPR profile. Although the process is kinetically limited, the influence of equilibrium conversion (i.e., x in CeO_{2-x}) is more pronounced at higher temperatures and is responsible for the asymmetry of the peak observed at $T > 1200$ K. It is only with the use of a forward/reverse reaction model that this part of the profile can be suitably reproduced.

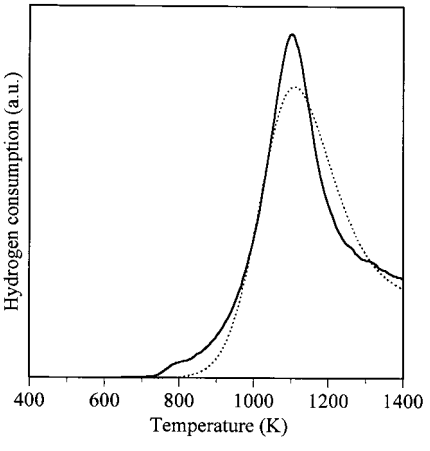

FIG. 5. Comparison of experimental TPR (solid line) and theoretical profile (dotted line) for LSA ceria in terms of H_2 conversion in arbitrary units ($1-y$ in model) versus temperature. For clarity, curves have been rescaled on a common basis to facilitate quantitative comparison.

The reliability of the model is quantitatively confirmed by the degree of conversion $x(T) = z(T)/2$ obtained from the model, depicted in Fig. 4 with the solid curve a. Figure 4 also depicts the theoretical $x(T)$ curves (vertical curves) corresponding to simulations analogous to MTPR experiments. The satisfactory agreement with the experimental data (filled circles and curve b) over a wide range of values for T confirms the validity of the model. No qualitative variations in the TPR profile are observed for specific surface area changes in the range 4–0.5 $m^2\ g^{-1}$.

3.3. *Kinetic Model of HSA Ceria Reduction*

In view of the observations in Section 3.1, it is reasonable to argue that the model developed for LSA ceria can be extended to HSA samples. This extension is not, however, obvious and requires some additional assumptions.

It has been pointed out that sintering plays a fundamental role in the reduction of HSA materials. A full description of this process is complex and involves several aspects. It is not only textural changes that occur during the sintering; there may also be a variation in the thermodynamic and kinetic properties induced by the process. However, it is worth pointing out that TPR data cannot be used for a detailed discrimination of the role of each of these phenomena, which are indeed closely related to each other. For this reason, a simplified formalization is assumed here, after which only surface area changes with temperature are considered.

If we bring together the experimental observations detailed in Section 3.1 and rule out a rate-limiting effect of oxygen diffusion,[1] the qualitative difference observed in the TPR of LSA and HSA ceria may be related to the

[1] It is possible to include the effect of diffusion. This, however, would make the model more elaborate without adding any new physical insight into the dynamics of the phenomenon and without appreciably modifying quantitatively the model results obtained by invoking spatial homogeneity. The inclusion of oxygen transport within the ceria lattice does not result only in a partial differential equation. Since the geometric length scales change with time (temperature), the resulting model for this phenomenon would be a moving-boundary value problem, which is much more cumbersome to deal with and physically unnecessary.

surface area changes occurring in the sample because of sintering. More precisely, the bimodal profile observed for HSA samples can be attributed to heterogeneity effects. The two-peak shape of HSA ceria is a consequence of the fact that nanocrystalline and bulk ceria possess different kinetic and thermodynamic properties. This conclusion is further supported by literature data on the equilibrium degree of reduction of nanocrystalline ceria, which reduces completely at relatively low temperatures because of a lower reduction enthalpy (1.84 eV vs 4.67 eV for bulk CeO_2) (15). The nonstoichiometry of nanocrystalline ceria is therefore several orders of magnitude greater than that of bulk ceria, which agrees with recent reports (15, 16).

Taking this as a working hypothesis, the phenomenology of HSA ceria reduction can be interpreted as follows: ceria nanocrystallites start to be reduced at lower temperatures ($T > 500$ K) than LSA samples and can be completely reduced thermodynamically even at these temperatures. This is responsible for the occurrence of the first peak. Simultaneously, the material undergoes structural modifications, and nanocrystallites modify progressively to bulk ceria. The reduction rate decreases at $T > 800$ K because nanocrystalline ceria is transformed into bulk ceria, which is characterized by different kinetic and equilibrium reduction properties. As a consequence, the shape of the HSA sample's first peak is due to the simultaneous effects of sintering dynamics and of kinetic limitations for the reduction of nanocrystallites. Conversely, the second peak follows the same thermodynamic and kinetic model developed in Section 3.2. Of course, this analysis refers to ideally clean samples free of impurities.

If we consider that reduction of nanocrystalline ceria implies mainly the removal of surface or near-surface oxygens, the reduction can be viewed as a process involving surface and bulk reduction in two successive steps. The surface area drop, which occurs under TPR conditions, causes a rapid variation in the reduction behavior, which originates the clear separation of the two contributions.

In a modeling framework, this premise leads us to consider HSA samples as formed by two phases, a nanocrystalline phase (referred to as the n-phase) and a bulk phase (b-phase). These two phases are also characterized by different thermodynamic and kinetic reduction properties. The bulk phase corresponds to the structure of LSA ceria and has the same properties, while for the n-phase it can be assumed that $x_{eq,n}(T) = 0.5$ under conditions typical for TPR experiments, as follows from the analysis reported by Hwang and Mason (15).

An estimate of the overall equilibrium value at any temperature is actually possible by repeating several MTPR experiments on HSA ceria. It is important to notice, however, that these results would be of no use unless accompanied by appropriate BET measurements since the equilibrium data for HSA ceria depend not only on the temperature but also on the surface area, and this dependence is difficult to describe in practice and theory. Moreover, the pretreatment process, or the presence of impurities, will severely affect the measurements, making it impossible to apply the results to different samples. Eliminating this lack of generality is not worth the effort required, and a lumped description is sufficient to reproduce the expected results, as we will show.

The transition from the n-phase to the b-phase is controlled by the textural changes induced by sintering. This is a continuous process dependent on temperature. In order to account for the fraction of the two phases at a given temperature, it is convenient to introduce a function ϕ, attaining values between 0 and 1, corresponding to the fraction of b-phase at a given temperature. It is reasonable to assume that ϕ depends exclusively on the specific surface area of the sample $\alpha(T)$ at temperature T, i.e., $\phi = \phi(\alpha(T))$. In particular, the function $\phi(\alpha)$ should attain values close to 0 for α of the order of magnitude of 50–60 $m^2\ g^{-1}$ or higher and values close to 1 for α around 2–3 $m^2\ g^{-1}$ or lower, and this function should monotonically decrease with α. For the sake of completeness, BET data for the surface area drop are depicted in Fig. 6. The continuous line corresponds to the curve fitting these data.

A candidate expression for $\phi(\alpha)$, which satisfies the properties discussed above is also depicted in Fig. 6, and it corresponds to the expression

$$\phi(\alpha) = 1 - \frac{[\exp(w_1\alpha) - 1]^4}{w_2 + [\exp(w_1\alpha) - 1]^4}, \qquad [11]$$

where w_1 and w_2 are two parameters (for the graph in Fig. 6, $w_1 = 0.04$, $w_2 = 40$). It should be observed that the functional form Eq. (11) is to some extent arbitrary,

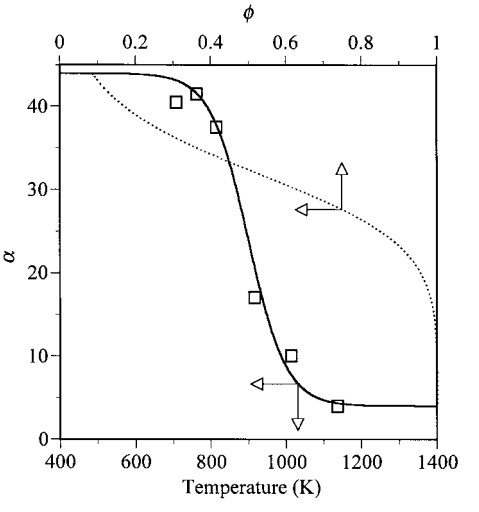

FIG. 6. Solid line: Specific surface area decay $\alpha(T)$ corresponding to a sample with an initial area of 44 $m^2\ g^{-1}$, obtained by BET measurements at several values of T (□ are experimental data). Dotted line: The $\phi(\alpha)$ versus α given by Eq. [11].

and this reflects the experimental difficulties in describing quantitatively the relative fraction of the two phases. The values of the parameters w_1, w_2 can be fine-tuned by comparison with experimental TPR profiles. The two phases (n- and b-phases) the material is formed of possess different kinetic and equilibrium properties. At any temperature the material is characterized by an overall equilibrium degree of reduction

$$z_{\mathrm{eq,tot}}(T) = \phi(\alpha(T))z_{\mathrm{eq,b}} + [1 - \phi(\alpha(T))]z_{\mathrm{eq,n}}, \quad [12]$$

where the subscripts b and n refer to the thermodynamic properties of bulk and nanocrystalline ceria, respectively. Equation [12] corresponds to the average of $z_{\mathrm{eq,b}}$ and $z_{\mathrm{eq,n}}$ weighted for degree of nanocrystallinity.

We can follow this superposition principle for developing the kinetic model by applying the same approach and basic assumptions discussed in Section 3.2. The material is characterized by the presence of two pseudo-species, corresponding to the maximum reduced oxide $CeO_{1.5}$ and to the unreduced oxide CeO_2. The state of reduction of the material can be described by introducing an overall degree of reduction z attaining values between 0 and 1. The time evolution of z depends on the reaction kinetics and on the transition from a totally nanocrystalline texture to a bulk one. The transition is simply accounted for by the behavior of the specific surface area with temperature and by the functional dependence of the degree of nanoncrystallinity on α.

Indicating as $k_{1\mathrm{b}}(T)$ the kinetic rate coefficient of the bulk phase (see Section 3.2) and as $k_{1\mathrm{n}}(T)$ that of the nanocrystalline phase, and introducing the dimensionless time θ, the overall dynamics of ceria reduction can be expressed as a linear combination of the kinetics of each phase, weighted by ϕ and $1-\phi$

$$\frac{dz}{d\theta} = h[\phi\,\tilde{k}_{1\mathrm{b}} + (1-\phi)\tilde{k}_{1\mathrm{n}}]\left(1 - \frac{z}{z_{\mathrm{eq,tot}}}\right), \quad [13]$$

where $h = h(T)$ is the normalized specific surface area, $h(T) = \alpha(T)/\alpha_{\mathrm{ref}}$, and the reference specific area is chosen as $\alpha_{\mathrm{ref}} = 3\ \mathrm{m^2\ g^{-1}}$ so that $\tilde{k}_{1\mathrm{b}}(T)$ coincides with the rate coefficient $\tilde{k}_1(T)$ obtained for LSA ceria. For $\tilde{k}_{1\mathrm{n}}(T)$ it is reasonable to use functional dependence on temperature analogous to that adopted for $\tilde{k}_1(T)$, but with a different set of values for the parameters a_3, b_3, a_4, b_4, T_{r3}. To avoid confusion, the parameters for $\tilde{k}_{1\mathrm{n}}(T)$ are marked by an overbar and are summarized in Table 1. The set of values reported in Table 1 was obtained by fitting the experimental data by constraining the model to reproduce the temperature location and intensity (expressed by the degree of reduction) of the first peak. The initial condition for Eq. [13] is obviously $z(\theta = 0) = 0$.

The kinetic model is completed by the hydrogen balance in the gas phase, which reads, in dimensionless form,

$$\frac{dy}{d\theta} = 1 - y - \frac{1}{2}\frac{\gamma}{\delta}\frac{dz}{d\theta}, \quad [14]$$

in analogy with Eq. [10] in Section 3.2 (with the same meaning for the dimensionless quantities γ and δ). Figure 7A shows the model prediction, obtained by integrating Eqs. [13] and [14] and plotting $1-y$ vs T, to be compared with the experimental data in Fig. 1. The comparison of the corresponding integral quantities, namely, the experimental and theoretical reduction degree x attained as a function of temperature, is depicted in Fig. 7B. As can be observed from these two figures, the model correctly predicts a slight decrease in the intensity of the second peak, as compared to the LSA sample case, while its shape and location remain unchanged. The decrease in intensity of the second peak is essentially a thermodynamic effect. In HSA samples, a fraction of the material has already been reduced before the rise of the second peak, and therefore the driving force $z - z_{\mathrm{eq,tot}}$ is smaller than in the pure LSA case, resulting in a lower second peak with respect to LSA samples.

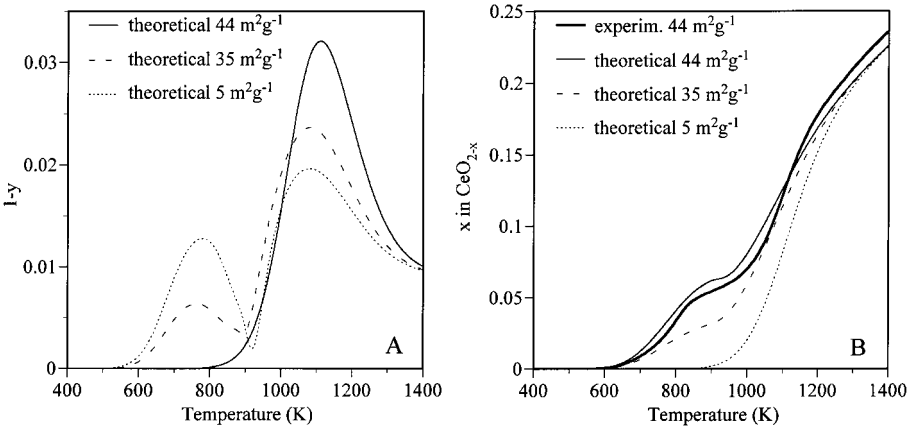

FIG. 7. (A) Theoretical TPR profiles ($1-y$ versus temperature) for ceria samples with different specific surface areas of 44, 35, and 5 $\mathrm{m^2\ g^{-1}}$. (B) Theoretical and experimental reduction degree x versus T corresponding to samples listed above.

A strictly quantitative agreement between model and experiments as regards the shape of the first peak is not possible and is ultimately of less practical utility owing to the presence of impurities affecting the shape of this peak. In fact, the shape of the first peak strongly depends on the material. Different HSA samples, purchased from different companies or pretreated in different ways, display great variability in the shape of the low-temperature peak, while its location remains practically unchanged. As a consequence, the parameters entering into the expression for $\tilde{k}_{1n}(T)$ and the functional form of $\tilde{k}_{1n}(T)$ itself are subject to a certain amount of variability, and the particular set listed in Table 1 is only indicative of an order of magnitude for these quantities. For all these reasons, it is of no interest to attempt to formulate a more complicated model to obtain a better reconstruction of the shape of the first peak. The lumped kinetic model proposed in this section is conceptually consistent with the physics of HSA ceria reduction and with the qualitative properties of TPR profiles observed experimentally. Moreover, the overall reaction properties, expressed by degree of reduction, are in satisfactory quantitative agreement with experimental data, as depicted in Fig. 7B. The actual degree of reduction after a complete TPR is in fact well predicted, and the differences from the experimental curve are only a consequence of the fitting of the equilibrium data and of the incomplete description of the equilibria for the nanocrystalline phase. To sum up, TPR of HSA ceria can be predicted with acceptable accuracy for integral quantities such as x, whereas the hydrogen consumption profile is more strongly affected by the simplifications of the model, and by its basic assumptions.

It is important to observe that the parametric form through which the fraction ϕ is expressed as a function of the surface properties of the material makes it possible to describe the dynamics of reduction of different ceria samples by means of Eq. [13], provided that the behavior of the specific surface area is known from BET measurements. In the light of the considerations of Section 3.1, it is to be expected that the intensity of the low-temperature peak will increase as the specific surface area of the material $\alpha(T_0)$ rises, and that the lowering of the second peak will be more pronounced, as previously discussed. It is worth pointing out that the dependence of the intensity of the first peak on the specific surface area is not linear due to the interplay between reduction kinetics and surface area changes. This can also be evinced from the model Eqs. [13] and [14]. The predictions of the model in this case are summarized by Fig. 7A, in which three different model samples are considered, each possessing different initial specific surface areas, namely, 5, 35, and 44 $m^2\ g^{-1}$, thus covering a range of values of practical interest. Qualitatively, model results are in agreement with the physical intuition, and it may be argued on a sound basis that the model, despite its formal simplicity, can be applied in a predictive way to different ceria samples in order to obtain a quantitative prediction of the reduction degree with temperature (the reduction degree x referring to the data of Fig. 7A is depicted in Fig. 7B), provided that the curve of surface area drop versus temperature is known.

4. CONCLUDING REMARKS AND OPEN PROBLEMS

In summary, we have shown that a two-step model involving surface and bulk reduction in different stages can be applied to represent the reduction profile of ceria under temperature-programmed conditions. The model is able to quantitatively predict the reduction profile of low surface area ceria at high temperature, but it is still too inaccurate to fully explain the details of the low-temperature reduction peak in the high surface area material. This is due to the intimate nature of the signal, which originates mainly from reduction of nanocrystalline material (or similarly from surface reduction of ceria) but which carries contributions from the presence of surface impurities, adsorption of hydrogen, and different reactivity of surface planes exposed. In addition, the surface area drop which inevitably accompanies ceria reduction in this temperature range adds to the complexity of the system. Nevertheless, the essential features of the bimodal TPR curve clearly emerge from this analysis. In particular, the following considerations can be made: the entire TPR profile is controlled by surface kinetics, although thermodynamic data are necessary to model the high-temperature profile. Diffusion is fast compared to surface processes over most of the temperature range investigated. The effects of diffusion can be considered at the beginning of reduction, during the onset of the first peak. The inclusion of oxygen diffusion into the model would solely modulate the shape of the low-temperature peak, and especially its rising front, without changing the conclusions derived from the model. Neglecting hydrogen adsorption and surface impurities, the model shows that the intensity of the first peak is proportional to the initial surface area, in line with previous findings.

A similar analysis is now under investigation to better explain the reduction profile of ceria doped with other elements.

ACKNOWLEDGMENTS

The authors are grateful to CNR and MURST for financial support. F.G. thanks the Ph.D. board (Processi Chimici Industriali) for financial support during her stay at the University of Udine. We also thank Grace Davison for providing high surface area ceria samples.

REFERENCES

1. Laachir, A., Perrichon, V., Badri, A., Lamotte, J., Catherine, E., Lavalley, J. C., El Fallah, J., Hilaire, L., LeNormand, F., Quéméré, E., Sauvion, G. N., and Touret, O., *J. Chem. Soc. Faraday Trans.* **87**, 1601 (1991).

2. Bernal, S., Calvino, J. J., Cifredo, G. A., Gatica, J. M., Perez Omil, J. A., and Pintado, J. M., *J. Chem. Soc. Faraday Trans.* **89**, 3499 (1993).
3. Padeste, C., Cant, N. W., and Trimm, D. L., *Catal. Lett.* **18**, 305 (1993).
4. El Fallah, J., Boujana, S., Dexpert, H., Kiennemann, A., Majerus, J., Touret, O., Villain, F., and LeNormand, F., *J. Phys. Chem.* **98**, 5522 (1994).
5. Cordatos, H., Ford, D., and Gorte, R. J., *J. Phys. Chem.* **100**, 18128 (1996).
6. Trovarelli, A., *Catal. Rev. Sci. Eng.* **38**, 439 (1996).
7. Kaspar, J., Fornasiero, P., and Graziani, M., *Catal. Today* **50**, 285 (1999).
8. Roozeboom, F., Mittlemeijer-Hazeleger, M. C., Moulijin, J. A., Medema, J., deBeer, V. H. J., and Gelling, P. J., *J. Phys. Chem.* **84**, 2783 (1980).
9. Yao, H. C., and Yao, Y. F. Y., *J. Catal.* **86**, 254 (1984).
10. Perrichon, V., Laachir, A., Bergeret, G., Fréty, R., Tournayan, L., and Touret, O., *J. Chem. Soc. Faraday Trans.* **90**, 773 (1994).
11. Bruce, L. A., Hoang, M., Hughes, A. E., and Turney, T. W., *Appl. Catal. A Gen.* **134**, 351 (1996).
12. Johnson, M. F. L., and Mooi, J., *J. Catal.* **103**, 502 (1987).
13. Conesa, J. C., *Surf. Sci.* **339**, 337 (1995).
14. Sayle, T. X. T., Parker, S. C., and Catlow, C. R. A., *Surf. Sci.* **316**, 329 (1994).
15. Hwang, J. H., and Mason, T. O., *Z. Phys. Chem.* **207**, 21 (1998).
16. Chiang, Y. M., Lavik, E. B., Kosacki, I., Tuller, H. L., and Ying, J. Y., *J. Electroceram.* **1**, 7 (1997).
17. Zotin, F. M. Z., Tournayan, L., Varloud, J., Perrichon, V., and Fréty, R., *Appl. Catal. A Gen.* **98**, 99 (1993).
18. Fierro, J. L. G., Soria, J., Sanz, J., and Rojo, J. M., *J. Solid State Chem.* **66**, 154 (1987).
19. James, A., and McNicol, B., *in* "Temperature Programmed Reduction for Solid Materials Characterization." Dekker, New York, 1986.
20. Steele, B. C. H., and Floyd, J. M., *Proc. Br. Ceram. Trans.* **72**, 55 (1971).
21. Inaba, H., and Tagawa, H., *Solid State Ionics* **83**, 1 (1996).
22. Kamiya, M., Shimada, E., and Ikuma, Y., *J. Ceram. Soc. Jpn.* **106**, 1023 (1998).
23. Martin, D., and Duprez, D., *J. Phys. Chem.* **100**, 9429 (1996).
24. Chiodelli, G., Flor, G., and Scagliotti, M., *Solid State Ionics* **91**, 109 (1996).
25. Fornasiero, P., Kaspar, J., and Graziani, M., *Appl. Catal. B Environ.* **22**, L11 (1999).
26. Perrichon, V., Laachir, A., Abouarnadasse, S., Touret, O., and Blanchard, G., *Appl. Catal. A Gen.* **129**, 69 (1995).
27. Bevan, D. J. M., and Kordis, J., *J. Inorg. Nucl. Chem.* **26**, 1508 (1964).